Electrical and thermal properties of structurally metastable iron-boron pairs in silicon

H. Nakashima, T. Sadoh, and T. Tsurushima
Department of Electrical Engineering, Kyushu University, 6-10-1 Hakozaki, Higashi-ku, Fukuoka 812, Japan
(Received 3 February 1994)

Structurally metastable iron-boron pairs in silicon have been detected using dark- or photocapacitance transient techniques combined with minority-carrier injection below 200 K. Five levels at $E_C-0.43$, 0.46, 0.52, and 0.54 eV and $E_V+0.53$ eV are observed as the metastable defects after the injection. The creation and annihilation behaviors of these defects by the injection are investigated in detail and discussed on the basis of the theory of recombination-enhanced defect reaction. The transmutations for respective defects are confirmed by isochronal anneals and the reaction kinetics are studied by isothermal anneals. These kinetic studies lead to a model for pair configurations responsible for these defect levels. The configuration-coordinate (CC) description for these metastable pairs is shown to account for all electrical and thermal properties. The CC model shows us why the metastability for the iron-boron pair cannot be observed in thermal equilibrium.

I. INTRODUCTION AND BACKGROUND

Iron is a principal contaminant during silicon device fabrication. Because of its high diffusion coefficient, iron is unstable even at room temperature and tends to form complexes with other impurities. Most iron-related defects are electrically active and therefore act to deteriorate device properties. Hence the properties of iron in silicon have been intensively investigated by many researchers.

Iron occupies a tetrahedral (T_d) interstitial site in the silicon lattice and acts as a donor ($Fe_i^{0/+}$) at $E_V+0.4$ eV.[1,2] In p-type silicon with group-III impurity, such as boron (B), aluminum (Al), gallium (Ga), and indium (In), mobile positively charged interstitial iron atoms (Fe_i^+) are captured by negatively charged substitutional acceptors (A_s^-) and consequently iron-acceptor (Fe_i-A_s) pairs are formed.[3,4] From a combination of electron paramagnetic resonance (EPR) and deep-level transient-spectroscopy (DLTS) results, the pairing formation, pair configuration, and energy-level structure have been comprehensively established.[1–5] In particular, the finding of bistable behaviors of Fe_i between the first nearest T_d site adjacent to A_s with ⟨111⟩-axis symmetry and the second T_d site with ⟨100⟩-axis symmetry gave rise to great interest in these pairs.[6,7] Recently, the bistable behaviors of Fe_i-A_s pairs have been studied in detail and become well established that the ⟨100⟩ configuration is metastable for Fe_i-Al_s and Fe_i-Ga_s pairs and the ⟨111⟩ configuration is metastable for Fe_i-In_s pair.[6–11] However, EPR results for the Fe_i-B_s pair show only the first nearest site Fe_i-B_s pair with ⟨111⟩ trigonal symmetry,[12] which is observed as a donor ($Fe_i^{+/++}$-B_s^-) at $E_V+0.1$ eV (Refs. 1 and 2) with DLTS. Hence the metastability on the Fe_i-B_s pair has not been found so far and has been left as an open question in the Fe_i-A_s pair system.

The pairing reaction of Fe_i with B_s is well described by the model[13] of the two-point charge Coulomb interaction between B_s^- and Fe_i^+ on the first nearest site, i.e., the pair binding energy E_B has been determined experimentally[14,15] close to 0.52 eV, which can be calculated from the model of two electrostatistically bounded point charges with the distance $r_1=2.35$ Å between the substitutional site and the first nearest T_d interstitial site. Thus energy-level structures for the isolated Fe_i^+ and the first nearest T_d site Fe_i^+ bounded to B_s^- can be illustrated as in Fig. 1(a) by using the configuration-coordinate (CC) description. This simple CC picture enables us not only

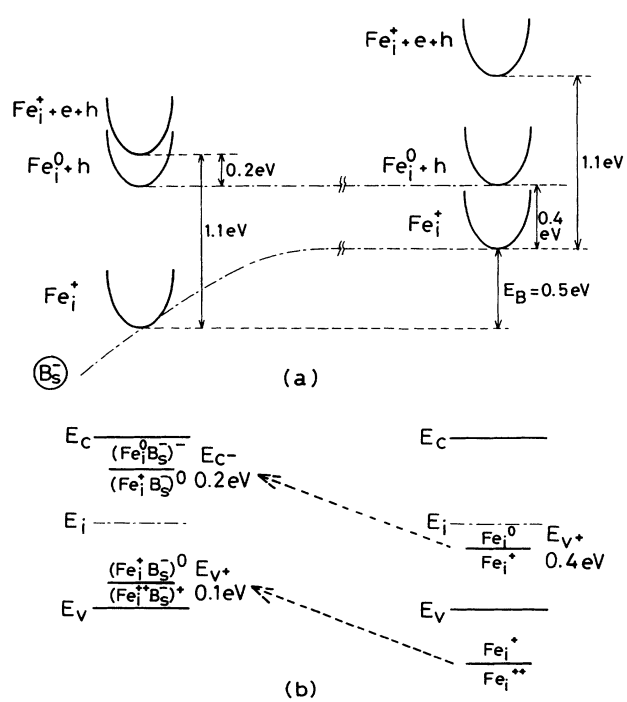

FIG. 1. (a) Simple configuration-coordinate diagram and (b) expected energy level for isolated Fe_i^+ and the first nearest T_d site Fe_i^+ bounded to B_s^-. The model is based on a Coulomb interaction potential between the two impurities.

 ©1994 The American Physical Society

to explain that the pair formation moves the Fe_i donor level ($Fe_i^{0/+}$) toward the conduction band, but also to expect that the first nearest Fe_i-B_s pair has an acceptor level ($Fe_i^{0/+}$-B_s^-) around $E_C-0.2$ eV, as shown in Fig. 1(b). Similarly, the donor level ($Fe_i^{+/++}$-B_s^-) at $E_V+0.1$ eV is explained by the model that the second donor level ($Fe_i^{+/++}$) lying in the valence band appears in the band gap as a result of the pair formation.

The acceptor level of the Fe_i-B_s pair has been reported as $E_C-0.23$ eV by Lemke[14] and as $E_C-0.29$ eV by Brotherton, Bradley, and Gill[16] using space-charge techniques. Recently, we have confirmed, using the photocapacitance transient technique, that the level at $E_C-0.29$ eV is due to the first nearest site Fe_i-B_s pair.[17] In addition, Gehlhoff and Rehse[18] have found a negative charge state of the trigonal Fe_i-B_s pair by using photoelectron paramagnetic resonance, which finds an acceptor level at $E_C-(0.25\pm0.05)$ eV. More recently, an acceptor level at $E_C-0.275$ eV for the Fe_i-B_s pair has been reported using Fourier transform spectroscopy and EPR.[19] From these results, it is confirmed that the acceptor level around $E_C-0.29$ eV is due to the first nearest-neighbor site Fe_i-B_s pair.

The Fe_i-B_s pair dissociates even below room temperature by minority-carrier injection from the n^+p junction.[15,20] This implies that Fe_i can sequentially jump from the first nearest site to another by absorbing the recombination energy. If a low level injection is carried out at such a low temperature that Fe_i cannot thermally migrate, it should be possible that Fe_i^+ atoms remain at structurally metastable sites bounded to B_s^-. Thus one would expect to create different pair configurations from the first nearest Fe_i-B_s pair. However, it is impossible to detect the donor levels of such metastable Fe_i-B_s pairs because the level positions become shallower than $E_V+0.1$ eV, corresponding to the first site pair, as inferred from the energy-level structure model shown in Fig. 1. By contrast, the acceptor levels of these metastable pairs should emerge between the acceptor level of the stable first nearest site Fe_i-B_s pair and the donor level of the isolated Fe_i. This means that the pair configurations are characterized by their level positions. Here it is noted that electron traps situated above intrinsic level E_i and hole traps below E_i must be detected by different space-charge techniques. We have already reported the observation of two acceptor-type hole trap levels of the metastable Fe_i-B_s pairs by using capacitance methods combined with minority-carrier injection at 150 K.[20] The energy levels have been determined to be $E_V+0.53$ (hereafter labeled $H2$) and 0.48 eV ($H3$), and it has been verified that the level $H2$ consists of two components due to trap $H2^*$ with a fast annihilation rate and trap $H2$ with a slow rate at around 220 K. Furthermore, we have recently found four metastable electron traps at $E_C-0.43$ ($E2$), 0.46 ($E3$), 0.52 ($E4$), and 0.54 eV ($E5$).[17,21] However, the detailed thermal properties have not been explored yet, and the pair configurations responsible for these metastable defects have not been assigned.

In this paper we present electrical and thermal properties of these metastable defects of Fe_i-B_s pairs in silicon and propose the pair configuration model for these defects. This paper is organized as follows. In Sec. II we present details of sample preparation and the principles and procedures for examining minority carrier traps. In Sec. III, first, we present the electrical properties of metastable Fe_i-B_s pairs; second, we examine the creation and the annihilation behavior of metastable pairs by minority-carrier injection; and third, we present isochronal and isothermal data for metastable defects. In Sec. IV we summarize the experimental results and propose the pair configuration model for metastable Fe_i-B_s pairs: traps $E2$, $H2$, and $E5$, which are assigned to Fe_i at the second, third, and fourth T_d sites in the vicinity of B_s, respectively. Moreover, we construct a CC model for the metastable Fe_i-B_s pair and show the reason why the metastability for the Fe_i-B_s pair cannot be observed in thermal equilibrium. Finally, migration of Fe_i in the vicinity of B_s is discussed using the theory of recombination-enhanced defect reaction, and the rationale for the pair configuration model is examined. Section V contains concluding remarks.

II. EXPERIMENTAL DETAILS

A. Principle for detecting minority-carrier traps

The principle for detecting an electron trap in the n^+p junction region is illustrated in Fig. 2(a). The technique is similar to that described in Ref. 22. The back surface of the reverse-biased diode is illuminated with light greater than the band gap energy, which causes the generation of electron-hole pairs in the back side region.

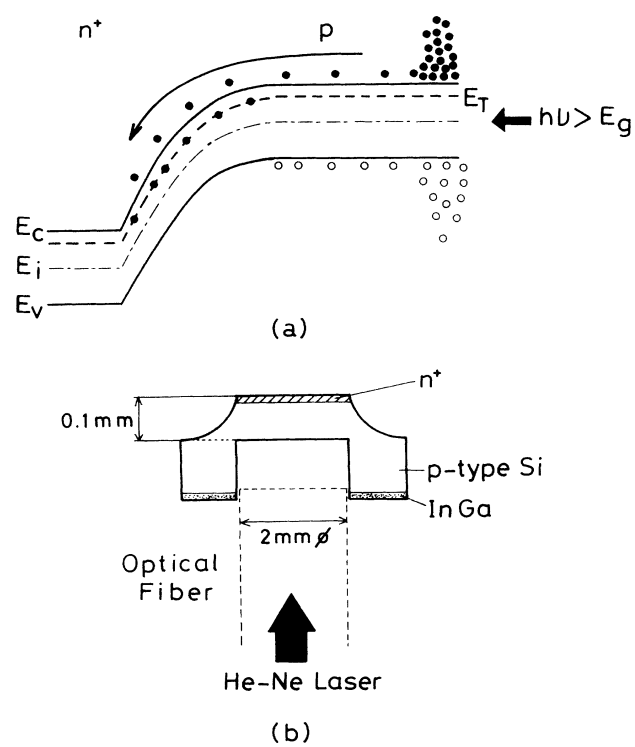

FIG. 2. (a) Principle and (b) sample structure for detecting an electron trap in the n^+p junction region.

The electron-hole pairs diffuse toward the reverse-biased region because of the concentration gradient. Since the reverse bias is a forward-bias direction for electrons and a reverse-bias direction for holes, only electrons can be introduced into the depletion region. When the optical source is switched off, electron emission from the electron trap occurs at the appropriate temperature; thus the emission process can be monitored by recording the capacitance change after the illumination. If the thickness of the p-type region is too thick or the Fe concentration too high, electrons cannot reach the edge of the depletion region because of recombination of electron-hole pairs in the p-type neutral region. Thus one requires a thin sample and low Fe concentration.

B. Sample preparation

The material used was float-zoned silicon crystal with a B concentration of 1.0×10^{14} cm^{-3} and a thickness of 0.5 mm. n^+p junctions were fabricated using a standard diffusion technique. The n^+p junction wafer was separated into several samples of 3.5×3.5 mm^2. After the back surface was coated with an aqueous solution of $FeCl_3$, the sample was sequentially heat treated in a vacuum at 900 °C for 3 h. The heat treatment was terminated by rapidly dropping the sample into diffusion pump oil. For the Fe-doped sample, a cylindrical cavity with diameter 2 mm was made from the back surface to the front and then chemically etched to obtain optical flatness. The effective sample thickness was about 0.1 mm. By mesa etching the n^+ layer and rubbing an In-Ga alloy on the back surface, an n^+p mesa-type diode with a junction area of 4 mm^2 was fabricated. The cross-section view of the sample is schematically shown in Fig. 2(b).

The Fe_i concentration in the sample just after quenching was estimated as 3×10^{13} cm^{-3} by DLTS, which agreed fairly well with the solubility data[23] of Fe_i at 900 °C. After sample storage at room temperature for a week following the anneal at 50 °C for 2 days to accelerate Fe_i-B_s pair formation, it was confirmed that the DLTS signal of $E_V+0.40$ eV for Fe_i was almost transformed to that of $E_V+0.10$ eV for the Fe_i-B_s pair.

C. Experimental procedures

Electron traps were observed by recording the capacitance change with $V_R=10$ V after having been illuminated with He-Ne laser light (the power was 10 mW, the wavelength 0.63 μm, and the absorption depth 3 μm), which was led to the cavity of the sample by an optical fiber, as shown in Fig. 2(b). Hole traps were observed by recording the capacitance change with $V_R=10$ V after having been applied zero bias in dark. Since the DLTS technique detecting a high emission rate was inadequate to investigate the metastable defects,[20] we used thermally stimulated capacitance (TSCAP) and single shot techniques[24] to observe the slow emission process at lower temperature. DLTS was only used for monitoring the donor level of the first nearest site Fe_i-B_s pair. Minority-carrier injection was accomplished using a constant current source in series with the diode. TSCAP or single shot measurement after the injection below 200 K was performed by the following procedure.

For TSCAP measurement, after the above procedure to fill traps with electrons or holes at a selected temperature, data of the junction capacitance C with $V_R=10$ V were stored in a computer for a temperature interval of 1 K during an upward thermal scan up to 200 K with heating rate $\beta=0.07$ K/s. Subsequently, the C data were also taken as a function of temperature T during a downward scan with the same β. The difference $\Delta C(T)$ between the upward data $C_{\rm up}(T)$ and downward data $C_{\rm down}(T)$, $\Delta C(T)=C_{\rm up}(T)-C_{\rm down}(T)$, as a function of T was obtained as a TSCAP signal. Thus the positive and negative signs of ΔC correspond to electron and hole traps, respectively. This is similar to the following single shot data.

The single shot measurement was performed by the following method. At a selected temperature, the capacitance $C(t)$ at time t with $V_R=10$ V, after the introduction of electrons or holes in the depletion region, was measured and the data were stored in a computer using a logarithmic sampling period in the time range $1-\sim10^3$ s. By subtracting the steady-state capacitance $C(\infty)$ from the data $C(t)$, the transient signal $\Delta C(t)=C(t)-C(\infty)$ was obtained as a function of time t. The data $\Delta C(t)$ were fitted to the following equation with two parameters of transient signal amplitude A and emission time constant τ:

$$\Delta C(t)=A\exp(-t/\tau)\ . \tag{1}$$

If the transient signal $\Delta C(t)$ consisted of several components, the values of A_i and τ_i for each component were evaluated by the nonlinear least-squares[25] fit of the measured signal $\Delta C(t)$.

III. RESULTS

A. Electrical properties of metastable Fe_i-B_s pairs

TSCAP and DLTS results before and after the minority-carrier injection at a forward current density J_F of 10 mA/cm^2 for 200 s at 150 K are shown in Fig. 3, where electron and hole trapping levels are labeled E and H, respectively. Only two levels $E1$ at $E_C-0.29$ eV and $H1$ at $E_V+0.10$ eV are observed before the injection, as shown by the solid lines in Fig. 3. The two levels are attributed to an amphoteric center of the first nearest Fe_i-B_s pair.[17,20] The emission rate for $E1$ will be shown later. No difference was found between the results under reverse bias and zero bias during sample cooldown. Moreover, despite changing the initial temperature prior to the sample cooldown, no level except $E1$ and $H1$ was ever detected. These results lead to a conclusion that the Fe_i-B_s pair does not show the bistability which has been found for Fe_i-Al_s, Fe_i-Ga_s, and Fe_i-In_s pairs. This conclusion is very consistent with that[12] from EPR.

By contrast, the injection at 150 K leads to a strong decrease of signals $E1$ and $H1$, as shown by the dashed lines in Fig. 3, and consequently, a broad signal in the range 140–190 K, which consists of four signals $E2$, $E3$, $E4$, and $E5$, and a signal $H2$ are detected. It has already been confirmed that the signal $H2$ is due to an accep-

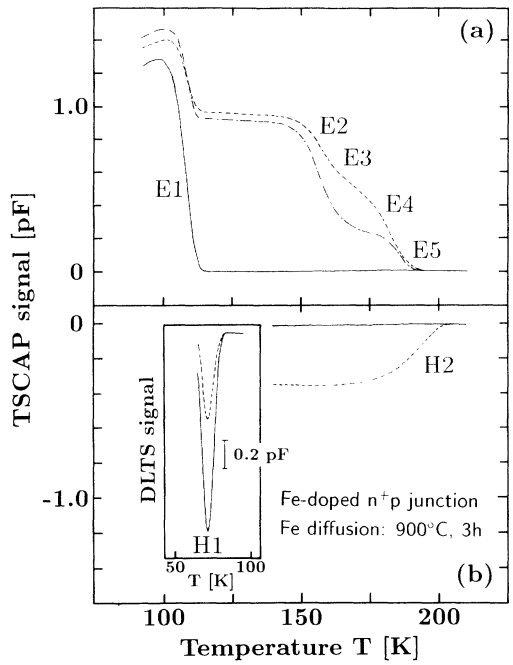

FIG. 3. TSCAP signals for (a) electron and (b) hole trapping levels for Fe-doped p-type silicon. The inset shows DLTS signals. Solid line, before injection; dashed line, after the injection of $J_F = 10$ mA/cm^2 for 200 s at 150 K; dash-dotted line, after annealing at 210 K for 10 min following the injection. The TSCAP results (a) and (b) were obtained after illuminating 0.63-μm light at 80 K and applying the zero bias at 130 K, respectively. The DLTS signals were generated under a gate setting $t_1/t_2 = 0.02/0.2$ ms. The reverse and filling biases are 10 and 0 V, respectively.

tor.[20] Similarly, the signals $E2$–$E5$ are due to acceptors, because the magnitude of the steady-state capacitance after electron emissions from these metastable defects is the same as that without these defects (before the minority-carrier injection). These results mean that Fe_i atoms at the first nearest sites adjacent to B_s atoms move to other sites by gaining the recombination energy and pairs with other configurations are created. Among these metastable defects, trap $E4$ is the most unstable defect and annihilates after annealing even at a temperature as low as 210 K, as shown by the dash-dotted line in Fig. 3(a). When the strong (longer time) injection was carried out, level $H3$ (0.48 eV), due to another metastable Fe_i-B_s pair, and $H4$ (0.40 eV), due to free Fe_i, were also observed. The detailed data on hole trapping levels $H2$ and $H3$ have been shown in our paper in Ref. 20.

Since the TSCAP technique was inadequate to evaluate the signal amplitude A and emission time constant τ for each level, the single shot technique was employed. Typical results for metastable defects created by the injection at 150 K are shown in Fig. 4, where (a) is the result for levels $E2$ and $E3$ obtained after the weak injection (10 s); (b) is the result for $E4$ and $E5$ obtained after the moderate injection (200 s); and (c) is the result for $H2$, $H3$, and $H4$ obtained after the strong injection (4000 s). The weak injection was used for the creation of levels $E2$, $E3$, and $E4$, and the moderate injection was for the creation of $E5$ and $H2$, in addition to the above levels.

Emission rates e_n with T^2 correction for electron trapping levels are shown in Fig. 5. The thermal emission activation energy for $E1$ was determined to be $E_C - 0.29$ eV, which was in full agreement with the result (dashed line) from the photocurrent DLTS measurement by Brotherton, Bradley, and Gill.[16] The emission rates for metastable defects were obtained at various temperatures after the following injections at 150 K and subsequent anneals for 10 min: $E2$, the weak injection and anneal at 225 K; $E3$, the weak injection and anneal at 210 K; $E4$, only the weak injection; and $E5$, the moderate injection and anneal at 210 K. It is noted that 210 and 225 K anneals are the procedures to perform the annihilation of $E4$ and $E3$, respectively. The energy levels for traps $E2$,

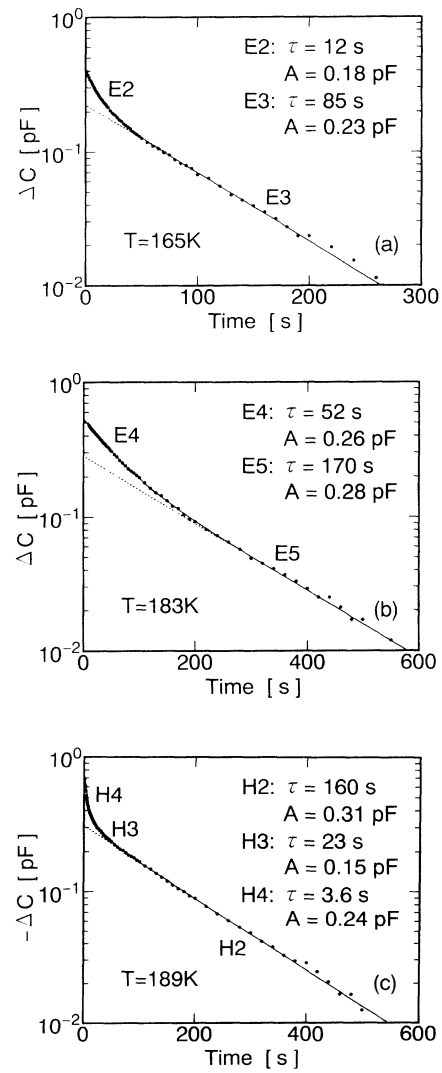

FIG. 4. Time variations in capacitance obtained after the injections of $J_F = 10$ mA/cm^2 for (a) 10 s, (b) 200 s, and (c) 4000 s at 150 K. The result (a) is obtained after the injection followed by the anneal for 10 min at 205 K. The solid lines represent the fitted curves. The positive and negative signs of ΔC correspond to electron and hole trapping levels, respectively.

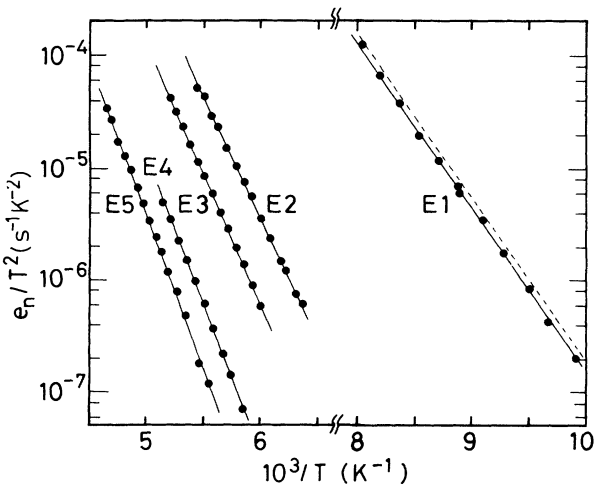

FIG. 5. Arrhenius plots of T^2 corrected thermal emission rates for electron trapping levels $E1$-$E5$. The measurements for respective metastable defects were executed after the following injections of $J_F = 10$ mA/cm^2 at 150 K and subsequent anneals for 10 min: $E2$, injection for 10 s and anneal at 225 K; $E3$, injection for 10 s and anneal at 210 K; $E4$, injection for 10 s without anneal; $E5$, injection for 200 s and anneal at 210 K. The dashed line shows the results from the photocurrent DLTS measurement by Brotherton, Bradley, and Gill (Ref. 16).

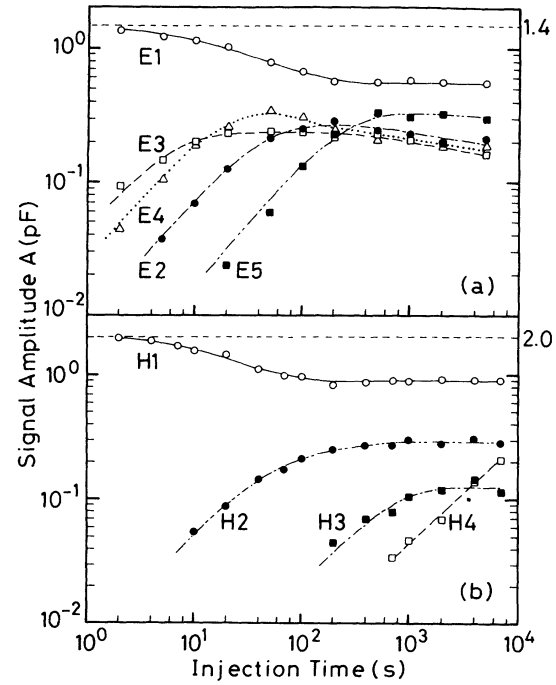

FIG. 6. Injection time dependence of the signal amplitude A of each defect under constant J_F of 10 mA/cm^2 at 150 K. (a) Results for electron trapping levels. (b) Results for hole trapping levels. The dashed lines represent A_{E1} and A_{H1} before the injection.

$E3$, $E4$, and $E5$ were determined to be $E_C - 0.43$, 0.46, 0.52, and 0.54 eV, respectively. Similarly, the hole trapping levels have been determined to be $E_V + 0.53$ ($H2$), 0.48 ($H3$), and 0.40 eV ($H4$).[20] Trap $H3$ has a small signal amplitude relative to the other metastable traps and is due to the rather distant Fe_i-B_s pair. Furthermore, the components of some other metastable defects are contained in the signal $H4$, as described in Ref. 20, but it is impossible to separate the components from the signal of free Fe_i because of almost the same emission rates. Thus we focus our attention on the creation and annihilation behavior for metastable defect levels $E2$–$H2$ hereafter. These metastable defect levels, of course, cannot be observed unless minority-carrier injection is carried out at a low temperature.

B. Creation and annihilation of metastable Fe_i-B_s pairs by minority-carrier injection

The amplitudes A of the signals $E1$–$E5$ and $H1$–$H4$ are shown in Fig. 6 as a function of injection time under the constant J_F of 10 mA/cm^2 at 150 K. The decreasing behavior of A_{E1} with the increase of the injection time shows a very good correlation with that of A_{H1}. We thus conclude that the two levels $E1$ and $H1$ are attributed to an amphoteric center of the first nearest site Fe_i-B_s pair. Upon increasing the injection time, levels $E3$, and $E4$, and $E2$ emerge sequentially, followed by the growth of $E5$ and $H2$; $H3$ begins to appear after the saturation of A_{E5} and A_{H2}. Finally, the signal $H4$, including the free Fe_i signal, can be detected. The time necessary for saturation is about 20 s for level $E3$, 50 s for $E4$, 100 s for $E2$, and 400 s for $E5$ and $H2$. For all metastable defect levels, except $H2$, the creation behaviors up to saturation can be represented by the first-order reaction, namely, $A(t) = A_{sat}[1 - \exp(-Rt)]$ (respective lines in Fig. 6), where R is the creation rate. The behavior for the level $H2$ is well fitted by two components rather than a single component. The rates R obtained for respective defects under $J_F = 10$ mA/cm^2 are shown in Fig. 7 as a function of injection temperature. In contrast to the creation behavior of level $H2$ at 150 K, those at 120 and 180 K could be well fitted by a single exponential form. Howev-

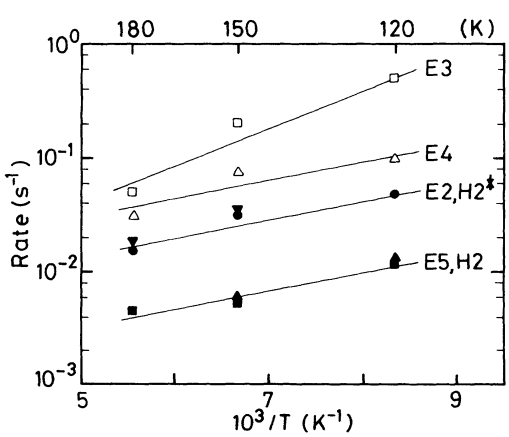

FIG. 7. Temperature dependence of the creation rate R for each defect under $J_F = 10$ mA/cm^2. ●, $E2$; □, $E3$; △, $E4$; ■, $E5$; ▼, $H2^*$; ▲, $H2$.

er, the rate obtained at 180 K is rather large, suggesting that the signal is mainly due to trap $H2^*$; the rate at 120 K is small, suggesting that the signal is mainly due to trap $H2$. Thus the rates for traps $H2^*$ and $H2$ are found to be similar to those for $E2$ and $E5$, respectively. The activation energy for trap $E3$ is about -0.06 eV and those for the other traps are about -0.03 eV. The negative activation energies imply that the recombination-enhanced defect reaction for each defect is athermal and the recombination energy is large relative to the thermal energy for surmounting the reaction barrier.

Next, we explored the injection temperature dependence of the signal amplitude A after the moderate injection ($J_F = 10$ mA/cm^2 for 200 s). The results are shown in Fig. 8. In the temperature range above 110 K, the creation of level $E2$ is not strongly dependent on the injection temperature. On the other hand, that of $E3$ increases with the increase of the temperature, while those of $E4$, $E5$, and $H2$ decrease. In other words, the injection at low temperature around 120 K elevates the creation of deeper levels $E4$, $E5$, and $H2$ and suppresses that of $E3$. Inversely, the injection at high temperature around 180 K suppresses the creation of their deeper levels and elevates that of $E3$.

However, the injection at lower temperature below 110 K suppresses the creation of all metastable defects; here the arrow in Fig. 8 indicates a temperature at which the Fermi level is located at the $H1$ level of $E_V + 0.10$ eV, which means that the charge state of the first nearest Fe_i-B_s pair becomes positive in the range below 110 K. This suggests that the first nearest Fe_i-B_s pair dissociates in the neutral state $(Fe_i^+\text{-}B_s^-)^0$, but does not dissociate in the positive state $(Fe_i^{++}\text{-}B_s^-)^+$. On the other hand, the metastable Fe_i-B_s pair should dissociate even at such a lower temperature because of the neutral state. Thus it is expected that the Fe_i atom, at the metastable site, can be moved by the injection at the lower temperature. Figure 9 shows the results for the injection recovery of metastable defects. The injection for creation and annihilation was performed at 120 and 85 K, respectively. As expected, signal amplitudes of levels $E2$–$H2$ decrease to equilibrium values at 85 K. The reactions for all levels

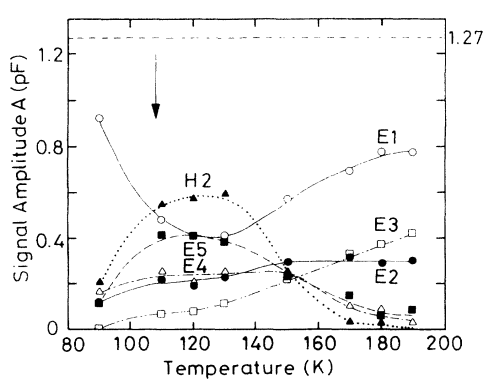

FIG. 8. Injection temperature dependence of the signal amplitude A of each defect under $J_F = 10$ mA/cm^2 for 200 s. The arrow indicates a temperature at which the Fermi level is located at the $H1$ level of $E_V + 0.10$ eV. ○, $E1$; ●, $E2$; □, $E3$; △, $E4$; ■, $E5$; ▲, $H2$.

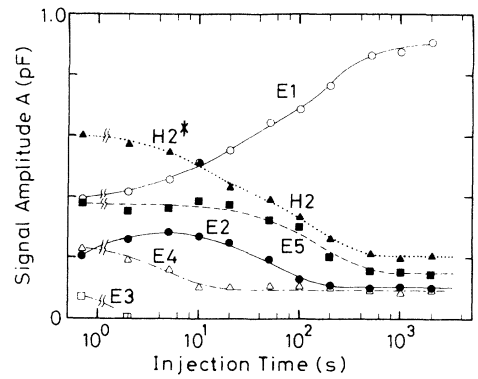

FIG. 9. Injection time dependence of the signal amplitude A of each defect under constant J_F of 10 mA/cm^2 at 85 K. The injection for creation of metastable defects was performed under $J_F = 10$ mA/cm^2 for 200 s at 120 K. ○, $E1$; ●, $E2$; □, $E3$; △, $E4$; ■, $E5$; ▲, $H2$.

$E2$–$E5$, except $H2$, are complete in about one order of injection time from the onset of the annihilation. The annihilation of level $H2$ proceeds slowly in the wide time range $1-10^3$ s, which suggests that the level $H2$ consists of two components due to trap $H2^*$ with a fast decay rate and $H2$ with a slow rate. This behavior is quite similar to the thermal annihilation behavior, as described in Sec. III C. Thus the recovery time is 2 s for trap $E3$, 10 s for $E4$, 30 s for $H2^*$, 200 s for $E2$, and 1000 s for $E5$ and $H2$. In particlar, recovery times of $E3$, $E4$, and $H2^*$ are very short, which strongly suggests that the origin of these traps is quite different from that of the stable traps $E2$, $E5$, and $H2$. These creation and annihilation behaviors will be discussed in Sec. IV. In this section we conclude that the recombination mode in the neutral state is necessary for dissociation of the Fe_i-B_s pair.

C. Thermal annihilation of metastable Fe_i-B_s pairs

In order to clarify the return paths for respective metastable Fe_i-B_s pairs, we investigated the annihilation behavior by isochronal anneals. Figures 10(a) and 10(b) show the results obtained from the isochronal anneals for 10 min at zero bias after the injections of $J_F = 10$ mA/cm^2 for 10 and 200 s at 150 K, respectively. For the case of weak injection [Fig. 10(a)], levels $E2$, $E3$, and $E4$ are created. Trap $E4$ vanishes at a very low temperature of 205 K. Its annihilation leads to the increase of traps $E2$ and $E3$, but does not lead to the increase of $E1$, implying that the thermal return path is $E4 \rightarrow E2$ and $E3$. Trap $E3$ annihilates at rather low temperature around 220 K. Since its annihilation causes the increase of $E1$, the path is $E3 \rightarrow E1$. Trap $E2$ shows stable behavior vanishing at around 240 K, and the path is clearly $E2 \rightarrow E1$.

For the case of moderate injection [Fig. 10(b)], levels $E5$ and $H2$ are also observed. Trap $E5$, as well as $E2$, is a thermally stable defect. All these traps $E2$–$E5$ rapidly disappear within 15–20 K from the onset of the annihilation. This suggests that the annealing kinetics are the first-order reactions. The annealing kinetics for respec-

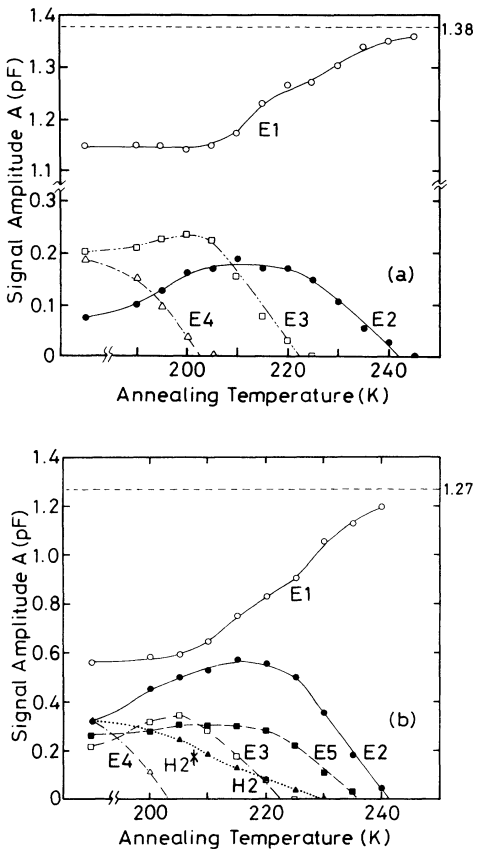

FIG. 10. Isochronal annealing data for metastable defect levels. The anneals were performed for 10 min under zero bias condition. (a) After the injection of $J_F = 10$ mA/cm^2 for 10 s at 150 K. (b) After the injection of $J_F = 10$ mA/cm^2 for 200 s at 150 K. ○, $E1$; ●, $E2$; □, $E3$; △, $E4$; ■, $E5$; ▲, $H2$.

tive traps will be shown later. The annihilation of level $H2$ proceeds slowly in the wide temperature range 200–230 K, indicating that the level $H2$ consists of two components due to trap $H2^*$ vanishing at around 215 K and trap $H2$ vanishing at 230 K. This observation is very consistent with our previous study,[20] namely, the isothermal annealing behavior of the level $H2$ shows a decay form with two time constants. The annihilation of traps $H2^*$ and $H2$ leads to the increase of trap $E2$, suggesting that traps $H2^*$ and $H2$ return to $E2$, and thus the path is probably $H2 \rightarrow H2^* \rightarrow E2$. Since the path for $E5$ is not clear from the isochronal data, we investigated the transmutation of $E5$ by the isothermal anneals at 230 K after the same injection at 120 K. The result is shown in Fig. 11. After unstable traps $E3$, $E4$, and $H2^*$ disappear within a few minutes, trap $H2$ decreases with an exponential form, and consequently the $E2$ decay form deviates from a single exponential; after the $H2$ annihilation terminates, trap $E2$ decays with an exponential form in spite of $E5$ annihilation. This means that the return path is $E5 \rightarrow E1$.

In order to clarify the jumping process for Fe_i^+ at each structurally metastable site, isothermal anneals under zero bias condition were explored around the

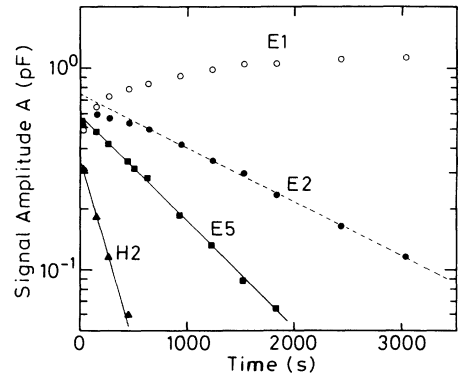

FIG. 11. Isothermal annealing data at 230 K for levels $E1$ (○), $E2$ (●), $E5$ (■), and $H2$ (▲). The injection was performed under $J_F = 10$ mA/cm^2 for 200 s at 120 K. The anneals were performed under zero bias condition.

transmutation temperature for each trap. The result for trap $E2$ is shown in Fig. 12. The annealing reaction is found to be the first order, as expected from the results of the isochronal anneals. Similarly, traps $E3$–$E5$ showed the simple exponential decay form. The decay rates R for traps $E2$, $E3$, $E4$, and $E5$ are plotted in Fig. 13 as a function of absolute temperature T. Our previous results[20] for traps $H2^*$ and $H2$ are also shown by the dashed lines in Fig. 13. They can be represented by the following expressions:

$$R_{E2} = 1.3 \times 10^{13} \exp(-0.75 \text{ eV}/kT) \text{ s}^{-1} , \quad (2)$$

$$R_{E3} = 1.9 \times 10^{14} \exp(-0.74 \text{ eV}/kT) \text{ s}^{-1} , \quad (3)$$

$$R_{E4} = 5.6 \times 10^{14} \exp(-0.70 \text{ eV}/kT) \text{ s}^{-1} , \quad (4)$$

$$R_{E5} = 1.1 \times 10^{13} \exp(-0.73 \text{ eV}/kT) \text{ s}^{-1} , \quad (5)$$

$$R_{H2^*} = 6.0 \times 10^{12} \exp(-0.65 \text{ eV}/kT) \text{ s}^{-1} , \quad (6)$$

$$R_{H2} = 3.9 \times 10^{12} \exp(-0.68 \text{ eV}/kT) \text{ s}^{-1} . \quad (7)$$

The rates except R_{E3} and R_{E4} seem to originate from the barrier to atomic motion of the Fe_i^+ atom from one

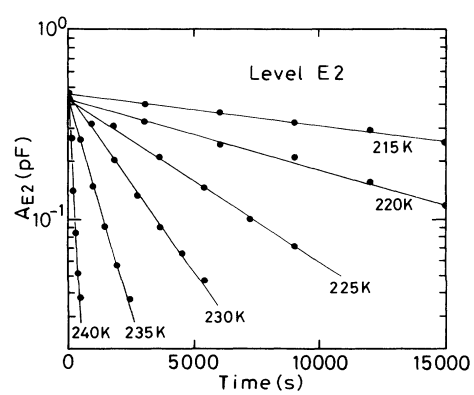

FIG. 12. Isothermal annealing data for level $E2$. The anneals were performed under zero bias condition.

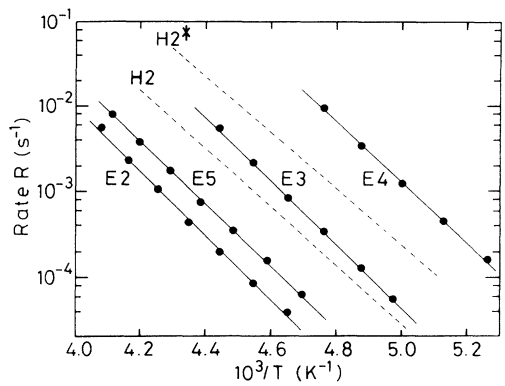

FIG. 13. Decay rates R of traps $E2$, $E3$, $E4$, and $E5$ as a function of reciprocal absolute temperature. The dashed lines represent R of traps $H2$ and $H2^*$ (Ref. 20).

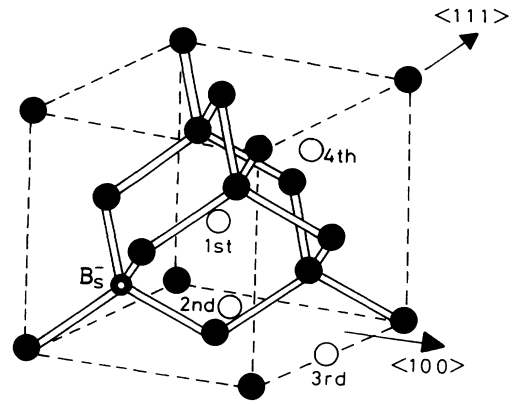

FIG. 14. Structure of silicon lattice. The black circle with the white center represents the substitutional B atom. The open circles represent the tetrahedral intersitial sites.

configuration to another because the preexponential factors are indeed in the range $10^{12}-10^{13}$ s^{-1} expected from a single jump process. The thermal activation energies E_D obtained are rather larger than that [0.66 eV (Ref. 26)] of free Fe_i^+, determined in the range 273–1343 K. These large E_D are probably related to the lattice strain in the vicinity of B_s. Thus we could make clear the return paths and reaction barrier heights E_D for metastable Fe_i-B_s pairs.

IV. DISCUSSION

The experimental results obtained in this study are summarized in Table I, where T_{an} is the annihilation temperature for 10-min anneals and E_P^{expt} the energy-level position obtained experimentally. On the basis of these results, we discuss the lattice position of Fe_i in the vicinity of B_s. The most stable sites for the occupancy of Fe_i should be T_d interstitial sites because of large atomic radius of Fe_i. Thus we can infer that thermally stable traps $E2$, $E5$, and $H2$ are attributed to Fe_i at T_d sites in the vicinity of B_s. Such T_d sites are shown in Fig. 14. The transition energies E_P^{calc} from Fe_i^0 to Fe_i^+ at these T_d sites are calculated using the configuration-coordinate description based on the simple ionic model by taking the acceptor level E_{P1}^{expt} of the first nearest pair as $E_C-0.29$ eV. The calculated results[20] E_P^{calc} are listed in Table I. Among the T_d sites shown in Fig. 14, Fe_i^+, at the second site of the ⟨100⟩ direction or at the fourth site of the ⟨111⟩ direction, is back to the first site by passing through a hexagonal ring of six atoms (H site), while Fe_i^+, at the third site, returns to the second site through an H ring. From this consideration and the correspondence of the calculated level position E_P^{calc} to the experimentally obtained position E_P^{expt}, traps $E2$, $H2$, and $E5$ can be assigned to the second, third, and fourth sites, respectively.

For the case of Fe_i^+-Al_s^- and Fe_i^+-Ga_s^- pairs, the first site pair with a ⟨111⟩ configuration is stable and the second site pair with a ⟨100⟩ configuration is metastable. Such metastable Fe_i^+-Al_s^- and Fe_i^+-Ga_s^- pairs can be observed by EPR and DLTS under the thermal equilibrium condition.[6–11] However, the metastable Fe_i-B_s pair is never observed unless the minority-carrier injection is carried out at low temperature, as described in Sec. III. This means that the difference ΔE_{12} between the total energies of Fe_i^+ at the first and second sites adjacent to B_s^- is much larger than ΔE_{12} for Al_s^- or Ga_s^-. The CC model for Fe_i at the first and second nearest sites in the Fe_i^+-B_s^- pair system, constructed from our experimental data, is shown in Fig. 15. The transition energies from Fe_i^+ to Fe_i^0 at the first and second sites are obtained as 0.81 (=1.1–0.29) eV and 0.67 (=1.1–0.43) eV, respectively. The difference $\Delta E_{P12}^{expt}=0.14$ eV between the two transition energies is considerably large relative to $\Delta E_{P12}^{calc}=0.07$ eV calculated on the assumption of a pure

TABLE I. Thermal return path, annihilation temperature T_{an}, reaction barrier height E_D, and level positions E_P^{expt} obtained from the experiment and E_P^{calc} from the calculation for metastable Fe_i-B_s pairs.

Trap		Path	T_{an} (K)	E_D (eV)	E_P^{expt} (eV)	E_P^{calc} (eV)	Site
$E1$					$E_C-0.29$		First T_d
$E2$	→	$E1$	242	0.75	$E_C-0.43$	$E_C-0.36$	second T_d
$E3$	→	$E1$	223		$E_C-0.46$		unidentified
$E4$	→	$E2,E3$	204		$E_C-0.52$		unidentified
$E5$	→	$E1$	238	0.73	$E_C-0.54$	$E_C-0.55$	fourth T_d
$H2^*$	→	$E2$	215		$E_V+0.53$		unidentified
$H2$	→	$E2$	230	0.68	$E_V+0.53$	$E_V+0.56$	third T_d

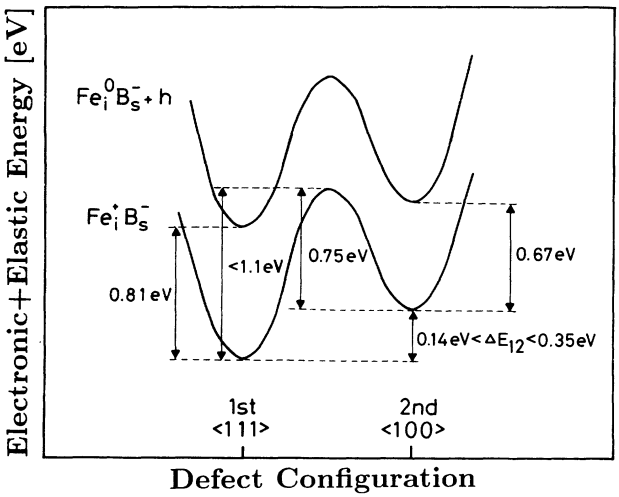

FIG. 15. Configuration-coordinate energy diagram for the first and second nearest Fe_i-B_s pairs. All the energies quoted on the CC diagram are deduced from the experimental study of the metastable-defect phenomenon.

Coulomb interaction, although excellent agreement between $\Delta E_{P12}^{\text{expt}}$ and $\Delta E_{P12}^{\text{calc}}$ has been found for the case of Fe_i-Al_s and Fe_i-Ga_s pairs.[7] This suggests that the elastic energy due to the strain effect originating from the B_s-Si bond length, in addition to the electronic energy due to the Coulomb interaction, must be taken into account for the lattice in the vicinity of the B_s atom. If the total energy of Fe_i^0 at the first site is equal to that at the second site, the difference $\Delta E_{P12}^{\text{expt}}=0.14$ eV corresponds to the total energy difference ΔE_{12} of Fe_i^+. Actually, the value of ΔE_{12} should be much larger than 0.14 eV because of the strain effect, but it should be less than 0.35 eV because the migration barrier height from the first site to the second site is less than 1.1 eV of the maximum recombination energy. Thus the value of ΔE_{12} is estimated as $0.14<\Delta E_{12}<0.35$ eV, which is rather consistent with the calculation result ($\Delta E_{12}=0.31$ eV) for the Fe_i^+-B_s^- pair done by Kimerling.[27] Even if the minimum value is used, the population ratio N_2/N_1 of the second site to the first site is calculated as 5×10^{-3} at 300 K. This explains why the second nearest Fe_i-B_s pair has never been detected so far in thermal equilibrium by EPR or junction capacitance technique. Similarly, ΔE_{14} is estimated as $0.25<\Delta E_{14}<0.37$ eV, and thus one would never also expect that the fourth Fe_i-B_s pair can be detected in thermal equilibrium.

The creation and annihilation behavior (Figs. 6–9) of metastable defects is based on the theory of recombination-enhanced defect reaction (REDR), which has been developed by Weeks, Tully, and Kimerling.[28,29] Since the creation rates observed for metastable Fe_i-B_s pairs show athermal properties (Fig. 7), the REDR rate R_{REDR} for a single jump process is given by

$$R_{\text{REDR}}=\eta R_R \ , \tag{8}$$

where η is an efficiency factor which relates to the fraction of recombination events which result in a successful reaction, and η increases as the recombination energy E_R and k_d/k_L ratio (k_d is the rate of energy flow within the defect molecule and k_L is the rate of energy loss to the lattice) increase; R_R is the recombination rate and is given by

$$R_R=\frac{(np-n_i^2)C_nC_p}{nC_n+pC_p} \ , \tag{9}$$

where n and p are the electron and hole concentrations, n_i the intrinsic carrier concentration, and C_n and C_p the respective capture coefficients.

Although it is not possible to measure the recombination rates and capture rates for respective levels in the range below 200 K, the limiting processes for the recombinations at respective levels should probably be probably electron capture processes because the creation rates for all these metastable defects are found to be roughly proportional to J_F. In fact, Lemke has reported the values of $C_p\approx3\times10^{-8}>C_n\approx10^{-8}$ cm^{3}s^{-1} at 90 K for the acceptor level of the first site Fe_i-B_s pair.[14] For the migration motion, the Fe_i^+ atom has the choice of moving into one of four nearest-neighbor T_d sites by passing through an H ring. The reaction path and migration probability p between the T_d sites in the vicinity of B_s are shown in Fig. 16. Thus the recombination-enhanced migration rate $R_{\text{REM}}^{i\to j}$ from the ith site to the adjacent jth site with $p^{i\to j}$ would be given by

$$\begin{aligned} R_{\text{REM}}^{i\to j}&=p^{i\to j}R_{\text{REDR}}^{i} \\ &\simeq p^{i\to j}\eta^i nC_n^i \ . \end{aligned} \tag{10}$$

The Fe_i^+ atom at the first site can migrate to the second site with $p=\frac{3}{4}$ and to the fourth site with $p=\frac{1}{4}$, which means that $R_{\text{REM}}^{1\to4}$ is three times smaller than $R_{\text{REM}}^{1\to2}$. For the creation of the third site, the jumping number of two times is required to move from the first to the third site, i.e., first → second → third, and Fe_i^+ at the second site migrates to the third site with $p=\frac{2}{4}$ and returns to the first site with $p=\frac{2}{4}$. This means that $R_{\text{REM}}^{1\to3}$ is four times smaller than $R_{\text{REM}}^{1\to2}$, assuming that R_{REDR} at the second site is equal to that at the first site. This explanation gives us the reason why the creation rates of traps $E5$ and $H2$ are about four times smaller than that

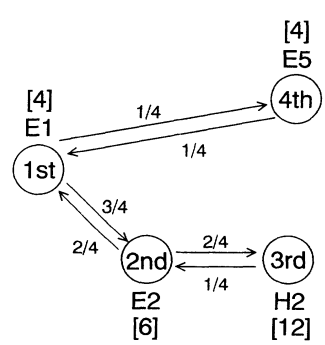

FIG. 16. Transmutation path and migration probability between T_d sites in the vicinity of B_s. The value in the square brackets represents the site number.

of $E2$ (Fig. 7).

For the case of the injection recovery shown in Fig. 9, the jumping number is precisely one time. The recovery from the second to the first site is done with $p=\frac{2}{4}$. By contrast, p from the fourth to the first site and from the third to the second site is $\frac{1}{4}$. Thus one would expect that the recovery times of Fe_i at the third and fourth sites are twice as long as that for the second site. However, the observed recovery times are about five times larger, indicating that R_{REDR} at $E5$ and $H2$ is somewhat low relative to $E2$. This is probably caused by lower C_n, E_R, or k_d/k_L ratio at traps $E5$ and $H2$ because of the deeper level positions.

On the other hand, the recovery of $E3$ is surprisingly fast, in spite of having almost the same energy level as trap $E2$. This means that η at trap $E3$ is much larger than that at $E2$. This finding strongly suggests that trap $E3$ is not due to the T_d site but due to the unstable site, e.g., the H site or the lattice strain-related site in the vicinity of B_s^- because the successful probability among the many attempts to jump at the T_d site is very small, while the migration probability at such unstable sites is rather high. Similarly, respective recovery times for traps $E4$ and $H2^*$ are about two orders of magnitude faster than those of $E5$ and $H2$ in spite of having almost the same energy levels. Thus we conclude that these unstable traps $E3$, $E4$, and $H2^*$ are not attributed to Fe_i atoms at the T_d sites.

Finally, we discuss the temperature dependence of the signal amplitudes in Fig. 8. As mentioned in Sec. III B, the injection at low temperature around 120 K enhances the creation of traps $E5$ and $H2$; inversely, the injection at high temperature around 180 K suppresses their creation. The behaviors are qualitatively explained as follows: If R_{REDR} at the first, second, third, and fourth T_d sites are equal, their population ratio should be proportional to the migration probability (the number of sites), i.e., 1st:2nd:3rd:4th=2:3:6:2 (see in Fig. 16). However, the population ratio is largely influenced by R_{REDR} at each site, which is a function of C_n, E_R, and the k_d/k_L ratio. The values of $R_{REM}^{1\to3}$ and $R_{REM}^{1\to4}$ measured at 120 K are four times lower than that of $R_{REM}^{1\to2}$, which means that R_{REDR} at the first and second sites are almost equal. By contrast, $R_{REM}^{4\to1}$ and $R_{REM}^{3\to2}$ are about two times lower than the rate expected from the migration probability, indicating that R_{REDR} at the third and fourth sites is half of that at the second site. Such decrease of the rates leads to enhancing largely the creation of Fe_i^+ at the third and fourth sites. On the other hand, $R_{REM}^{1\to2}$ and $R_{REM}^{1\to4}$ at 180 K decrease to about $\frac{1}{4}$ of those at 120 K, and the creation of $H2$ cannot be observed. The facts suggests that R_{REDR} at the first and second sites becomes considerably small, which explains the great increase of the first site and the great decrease of the third site. However, the large decrease of the fourth site cannot be explained by such decrease of R_{REDR}. Another possible explanation is that the decrease of $E5$ is associated with the increase of $E3$, namely, the transmutation path for $E5$ is $E1 \rightleftarrows E3 \rightleftarrows E5$. If so, trap $E3$ may be attributed to the H site of the middle point between the first and fourth T_d sites. Similarly, trap $H2^*$ may be attributed to the H site between the second and third sites. In order to comprehend quantitatively the creation behaviors of respective metastable traps, more detailed knowledge on the lattice sites of unstable traps and R_{REDR} at respective sites would be necessary.

Although lattice positions of unstable traps $E3$, $E4$, and $H2^*$ are ambiguous, the assignments of traps $E2$, $E5$, and $H2$ as T_d sites can explain rather well all electrical and thermal properties investigated in this studies. Therefore, we strongly suggest that traps $E2$, $H2$, and $E5$ are due to Fe_i atoms at the second, third, and fourth T_d sites adjacent to B_s atoms, respectively.

V. CONCLUSIONS

Observations of metastable iron-boron pairs in silicon have been reported using transient capacitance techniques combined with minority-carrier injection. Five levels at $E_C-0.43$, 0.46, 0.52, and 0.54 eV and $E_V+0.53$ eV are observed as metastable defects after the injection below 200 K. From the investigation of their electrical and thermal properties, it has been proposed that levels at $E_C-0.43$ eV, $E_V+0.53$ eV, and $E_C-0.54$ eV originate from the electronic transition $Fe_i^{0/+}$ of interstitial iron at the second, third, and fourth nearest tetrahedral interstitial sites adjacent to negatively charged substitutional boron atoms, respectively. The pair configuration model explains rather well the creation behaviors by the injection. The thermal annihilation rates for these levels show a single jumping process of interstitial iron from one configuration to another. The reaction barrier heights are determined to be 0.75 (second site), 0.68 (third), and 0.73 eV (fourth), which are rather large relative to free Fe_i. This seems to be related to the lattice strain in the vicinity of boron. The other levels show unstable thermal and injection annihilation behaviors, which suggest that these levels are attributed to unstable sites such as hexagonal sites or lattice strain-related sites in the vicinity of boron atoms.

ACKNOWLEDGMENTS

We are very grateful to Professor H. Kitagawa of Fukuoka Institute of Technology and Professor M. Suezawa of Tohoku University for their valuable discussion. We are very thankful to Professor W. Gehlhoff for his helpful suggestion and for private communication of his EPR work on metastability of the iron-acceptor pairs in silicon. We would like to thank Nippon Steel Corporation and Shin-Etsu Handotai Co., Ltd. for supplying the silicon wafers.

[1]K. Graff and H. Pieper, J. Electrochem. Soc. **128**, 669 (1981).
[2]K. Wünstel and P.Wagner, Appl. Phys. A **27**, 207 (1982).
[3]H. H. Woodbury and G. W. Ludwig, Phys. Rev. **117**, 102 (1960).
[4]G. W. Ludwig and H. H. Woodbury, in *Solid State Physics*, edited by F. Seitz, D. Turnbull, and H. Ehrenreich (Academic, New York, 1962), Vol. 13, p. 223.
[5]C. A. J. Ammerlaan, Solid State Phenom. **6&7**, 591 (1989).

[6]A. Chantre and D. Bois, Phys. Rev. B **31**, 7979 (1985).

[7]A. Chantre and L. C. Kimerling, in *Defects in Semiconductors 14,* edited by H. J. von Bardeleben, Materials Science Forum Vols. 10–12 (Trans. Tech., Aederomannsdorf, Switzerland, 1986), p. 387.

[8]J. J. van Kooten, G. A. Weller, and C. A. J. Ammerlaan, Phys. Rev. B **30**, 4564 (1984).

[9]W. Gehlhoff, K. Irmscher, and U. Rehse, in *Defects in Semiconductors 15,* edited by G. Ferenczi, Materials Science Forum Vols. 38–41 (Trans. Tech., Aederomannsdorf, Switzerland, 1989), p. 373.

[10]W. Gehlhoff, P. Emanuelsson, P. Omling, and H. G. Grimmeiss, Phys. Rev. B **41**, 8560 (1990).

[11]H. Takahashi, M. Suezawa, and K. Sumino, Phys. Rev. B **46**, 1882 (1992).

[12]W. Gehlhoff and K. H. Segsa, Phys. Status Solidi B **115**, 443 (1983).

[13]H. Conzelmann, K. Graff, and E. R. Weber, Appl. Phys. A **30**, 169 (1983).

[14]H. Lemke, Phys. Status Solidi A **64**, 215 (1981).

[15]L. C. Kimerling and J. L. Benton, Physica **116B**, 297 (1983).

[16]S. D. Brotherton, P. Bradley, and A. Gill, J. Appl. Phys. **57**, 1941 (1985).

[17]H. Nakashima and T. Sadoh, in *Defect Engineering in Semiconductor Growth, Processing and Device Technology,* edited by S. Ashok, J. Chevallier, K. Sumino, and E. Weber, MRS Symposia Proceedings No. 262 (Materials Research Society, Pittsburgh, 1992), p. 555.

[18]W. Gehlhoff and U. Rehse, in *Defect Engineering in Semiconductor Growth, Processing and Device Technology* (Ref. 17), p. 507.

[19]S. Ghatnekar-Nilsson, M. Kleverman, P. Emanuelsson, and H. G. Grimmeiss, in *Defects in Semiconductors 17,* edited by H. Heinrich and W. Jantsch, Materials Science Forum Vols. 143–147 (Trans. Tech., Aedermannsdorf, Switzerland, 1994), p. 171.

[20]H. Nakashima, T. Sadoh, and T. Tsurushima, J. Appl. Phys. **73**, 2803 (1993).

[21]H. Nakashima, T. Sadoh, and T. Tsurushima, in *Defects in Semiconductors 17* (Ref. 19), p. 1191.

[22]S. D. Brotherton, J. Appl. Phys. **55**, 3636 (1984).

[23]E. Weber and H. G. Riotte, J. Appl. Phys. **51**, 1484 (1980).

[24]H. G. Grimmeiss and C. Ovrén, J. Phys. E **14**, 1032 (1981).

[25]R. Langfeld, Appl. Phys. A **44**, 107 (1987).

[26]H. Nakashima and K. Hashimoto, in *Defects in Semiconductors 16,* edited by G. Davis, G. G. Deleo, and M. Stavola, Materials Science Forum Vols. 83–87 (Trans. Tech., Aedermannsdorf, Switzerland, 1992), p. 227; H. Nakashima, T. Sadoh. H. Kitagawa, and K. Hashimoto, in *Defects in Semiconductors 17* (Ref. 19), p. 761.

[27]L. C. Kimerling, M. T. Asom, J. L. Benton, P. J. Drevinsky, and C. E. Caefer, in *Defects in Semiconductors 15* (Ref. 9), p. 141.

[28]J. D. Weeks, J. C. Tully, and L. C. Kimerling, Phys. Rev. B **12**, 3286 (1975).

[29]L. C. Kimerling, Solid-State Electron. **21**, 1391 (1978).